COMMUNICATION

Two-Dimensional TiO_2 Inverse Opal with a Closed Top Surface Structure for Enhanced Light Extraction from Polymer Light-Emitting Diodes

*Woo Jin Hyun, Hang Ken Lee, Sang Soon Oh, Ortwin Hess, Choon-Gi Choi, Sang Hyuk Im, and O Ok Park**

Light-emitting diodes (LEDs), including organic LEDs and polymer LEDs, have been studied intensively for use in displays and interior lighting due to their promising advantages of high efficiency, high contrast ratio, long lifetime and low power consumption.[1,2] However, in a conventionally structured LED, less than 20% of the generated light is emitted as useful radiation.[3,4] Not surprisingly, the improvement of light extraction efficiency is currently considered to be one of the most important issues for LED research. A variety of strategies have been suggested towards this end, including modified substrates, microlenses, silica microspheres, silica aerogels[5–8] and two-dimensional (2D) photonic crystals (PhCs).[9–11]

Inverse opals (IO)[12,13] are one of the most promising approaches to realization of a 2D PhC structure.[14,15] To date, most of the reported 2D IOs have been fabricated with open top-surface structures. However, it is difficult to deposit thin layers for fabrication of LEDs onto the mesoporous structure and to attain a high refractive index contrast to raise efficient diffraction of waveguided light.[16] Moreover, it is desirable that organic materials do not infiltrate into the air void when IOs with air pockets are inserted between the multiple-layered structure. Thus, it is very challenging to fabricate a 2D IO with closed top-surface structure for further application.

Here, we demonstrate experimentally and numerically the enhanced light extraction efficiency of a polymer LED in which, for the first time, a 2D TiO_2 IO structure is inserted between the glass and anode electrode. Unlike conventional 2D IO structures, the 2D TiO_2 IO structures with closed top-surface have a thin flat film on top, where thin layers for fabrication of LEDs can conveniently be added easily onto the structure even via a solution process like spin-coating. For enhancing the light extraction from LEDs, this approach is very useful since a 2D PhC pattern can be easily obtained by adopting a simple colloidal assembly technique and sol-gel method. Furthermore, it is convenient to control the period of the 2D PhC pattern just by varying the size of the opal template nanoparticles used in the colloidal assembly process. To estimate the light extraction efficiency enhancement of the 2D TiO_2 IO structure and investigate the far-field radiation pattern with respect to the periods of the 2D TiO_2 IO structure, we performed three-dimensional finite-difference time-domain (3D-FDTD) simulations.[17] Finally, we confirmed that the 2D TiO_2 IO structure enhanced the extraction efficiency by comparing the measured enhancement of the fabricated LED devices with that simulated.

Figure 1 shows a schematic diagram of the fabrication of the 2D TiO_2 IO with a closed top-surface structure. The fabrication started with an opal monolayer template using polystyrene (PS) nanoparticles prepared by emulsifier-free emulsion polymerization.[18] Using 270 nm PS nanoparticles, an opal monolayer template was fabricated on glass by a confined convective assembly, which is a very effective way to fabricate 2D colloidal crystal films.[19] Briefly explaining the process, a 0.5 wt.-% 270 nm PS colloidal particles suspension in water containing a polyvinylpyrrolidone (PVP: $M_w = 55\,000$) weight fraction of 7.5×10^{-5} was prepared. An aqueous suspension (about 50 μL) of colloidal

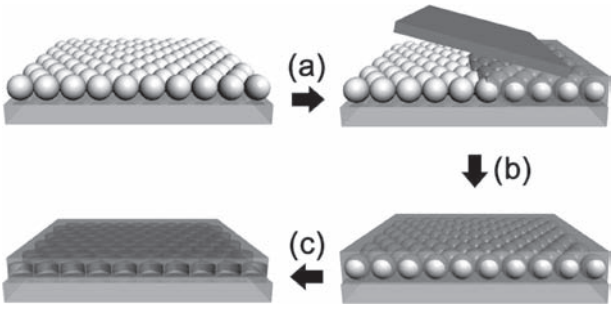

Figure 1. Steps in the fabrication of 2D TiO_2 IO with closed top-surface. a) An opal monolayer template of PS nanoparticles was fabricated on glass by a confined convective assembly. b) The PS template was infiltrated with a TiO_x sol solution by a doctor blade technique. c) The PS nanoparticles of the template were removed by calcination.

W. J. Hyun, Dr. H. K. Lee, Prof. O. O. Park
Department of Chemical and Biomolecular Engineering
(BK21 Graduate Program)
Korea Advanced Institute of Science and Technology
335 Gwahangro, Yuseong-gu, Daejeon, 305–701, Republic of Korea
E-mail: ookpark@kaist.ac.kr
Dr. S. S. Oh, Prof. O. Hess
Department of Physics
Imperial College London
South Kensington Campus, London SW7 2AZ, UK
Dr. C.-G. Choi
Convergence and Components & Materials Research Laboratory
Electronics and Telecommunications Research Institute
138 Gajeongro, Yuseong-gu, Daejeon, 305–700, Republic of Korea
Dr. S. H. Im
KRICT-EPFL Global Research Laboratory
Advanced Materials Division
Korea Research Institute of Chemical Technology
19 Sinseongno, Yuseong-gu, Daejeon, 305–600, Repubic of Korea

DOI: 10.1002/adma.201004660

particles was inserted into the gap between two glass substrates. One of the two glass substrates (the back substrate) was connected to a dipping machine to control the lift-up rate and the other glass substrate (the front substrate) was fixed. The back glass substrate was then raised at a rate of 19.5 μm s^{-1}, while adding an air flow towards the meniscus that was formed at the interface of the glass substrate and the colloidal suspension. The colloidal particles then assembled into a monolayer on the back substrate. It has been reported that the presence of water-soluble polymer (PVP) in the suspending medium results in high quality colloidal crystals with enhanced physical stability owing to the formation of the polymer bridges bonding each particle to neighboring particles and to the glass substrate.[20] In addition to the important role of PVP in the formation of good colloidal crystals, it has another advantage for fabricating IOs: when the colloidal particles are well connected to each other by PVP bridges, no additional step such as thermal annealing[21] is needed to obtain high quality IOs. After fabrication, the opal monolayer template was covered with the TiO_x sol solution by a doctor blade technique. Unlike conventional 2D IO structures, the 2D TiO_2 IO had a flat top-surface without significant cracks. If the deposited film were thick, there would be large cracks and the structure would break due to the shrinkage of TiO_2 during calcination.[12] In this respect, the deposition thickness is a critical factor for fabricating the 2D TiO_2 IO with a closed top-surface structure. After evaporating the solvent, PS nanoparticles were removed by calcination. We put the samples into a furnace and increased the temperature from room temperature to 500 °C at the rate of 1 °C min^{-1} and kept it at that temperature for 2 h. This calcination step not only removes the PS opal monolayer template but also transforms the amorphous phase of the TiO_2 into the crystalline phase, leading to an increase of the refractive index and mechanical property.

Figure 2 shows scanning electron microscopy (SEM) images of the fabricated 2D TiO_2 IOs with closed top-surface structure. From the SEM images, we can notice that a very thin TiO_2 film (30–40 nm) covers the void spaces of the IO, so that the surface is flat without any significant cracks. Because the thin film of TiO_2 is transparent, from the top view image in Figure 2a it can be seen that the structure replicated well from an opal monolayer template composed of 270 nm PS spheres. As shown in the inset of Figure 2a, voids look elliptical or almost rectangular in the cross-sectional view, which indicates the 2D IO was fabricated with cylindrical voids. The deformation from the spherical shape of the nanoparticle template into the cylindrical shape is attributed to the shrinkage of TiO_2 during calcination[12] as a consequence of the removal of volatile components like water and alcohol. It is interesting to see that this shrinkage occurs in the vertical direction but not in the horizontal direction. This implies that the TiO_2 material is stuck to the glass substrate firmly. The diameter of the voids remains almost the same and the height of the voids is decreased by about 50% as compared with the original diameters of the nanoparticles of the opal monolayer template. We obtained various periods of 2D TiO_2 IOs with closed top-surface structure easily by varying the size of the PS nanoparticles used in the colloidal assembly process for the opal monolayer template. Figures 2b and 2c show 2D TiO_2 IOs with closed top-surface structure fabricated from the opal monolayer template composed of 360 and 450 nm PS spheres, respectively.

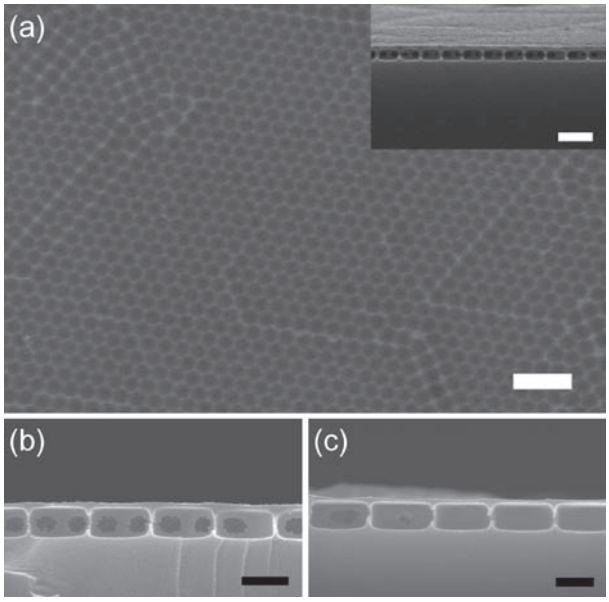

Figure 2. SEM images of fabricated structures. a) Top and cross-sectional (inset) views of the 2D TiO_2 IO with closed top-surface structure prepared from 270 nm PS opal template. b,c) Cross-sectional views of the structures prepared from, respectively, 360 and 450 nm PS opal monolayer templates. The structure is comprised of a well-ordered 2D hexagonal array of air voids and covered with a thin flat film on top. Scale bars: a) 1 μm (500 nm for inset); b,c) 300 nm.

Prior to fabricating the polymer LED with insertion of the 2D TiO_2 IO between the glass and anode electrode, we numerically calculated the enhancement of the structure using the 3D-FDTD method. This requires modeling of a huge number of dipole sources with random orientations, locations and phases in an active area. In principle, one may either include sufficiently many random dipoles and calculate the total output power in a single FDTD run[22,23] or perform several FDTD simulations with a few dipole sources.[24] Here we used the second approach, since it avoids interference between dipole sources in each FDTD run therefore makes the problem simpler and clearer. To obtain the average power, we used the following equation

$$\left\langle \left|\vec{E}\right|^2 \right\rangle = \frac{1}{3}\left[\left\langle \left|\vec{E}_x\right|^2 \right\rangle + \left\langle \left|\vec{E}_y\right|^2 \right\rangle + \left\langle \left|\vec{E}_z\right|^2 \right\rangle\right] \quad (1)$$

where E is the electric field and the subscripts x, y, z denote the orientations of the dipole sources. The structure used in our calculation is shown in **Figure 3**a. We modelled the 2D hexagonal array of cylindrical air holes within a TiO_2 layer on top of the anode electrode. The lattice constant of the PhC varies from 270 to 450 nm, which equals the diameter of the PS nanosphere templates. The diameter of the air cylinder is set to equal to the lattice constants and the height is set as one half of the diameter. Therefore, the total thickness of the TiO_2 IO layer ranges from 170 to 260 nm because there is a 35 nm thin TiO_2 film between the air holes and the cathode electrode. In order to model dipole sources with random position and orientation, we firstly set the eight locations in a unit cell, as shown in Figure 3b, and then performed simulations three times for

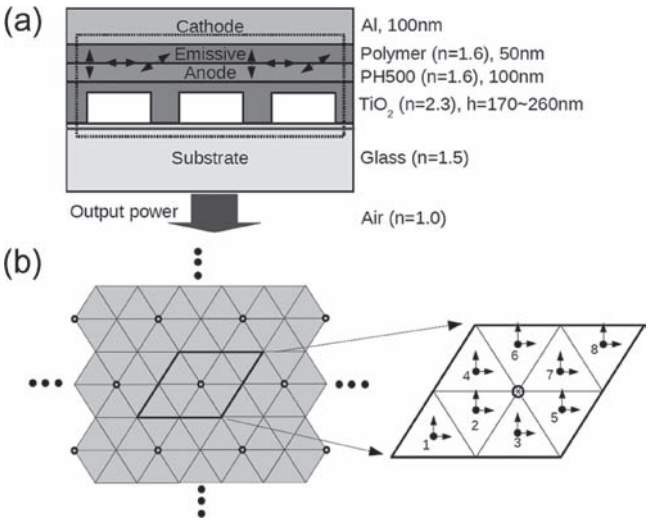

Figure 3. a) Schematic cross-section of the 2D TiO_2 IO structure used in the 3D FDTD calculations. The positions of electric dipole sources are marked with arrows. The dotted line denotes FDTD simulation space and the line below the 2D TiO_2 IO structure is the monitor plane. b) A unit cell and the location of the dipole sources. The total size of simulation is about $10 \times 10\ \mu m^2$.

the dipole sources with three orientations (x, y, and z) at each position. From the calculated far-field electric field, we calculated the extraction efficiency enhancement defined as:

$$\eta(\omega) = \frac{\int_\Omega \vec{S}_{IO}(\omega, \theta, \varphi) \cdot \hat{n} d\Omega}{\int_\Omega \vec{S}_{ref}(\omega, \theta, \varphi) \cdot \hat{n} d\Omega} = \frac{\int_\Omega \left|\vec{E}_{IO}(\omega, \theta, \varphi)\right|^2 d\Omega}{\int_\Omega \left|\vec{E}_{ref}(\omega, \theta, \varphi)\right|^2 d\Omega} \quad (2)$$

where $\vec{S}$ is the Poynting vector for direction of (θ, ϕ), ω is the angular frequency of light, Ω is the solid angle where the output power is measured, and the subscripts IO, ref mean the polymer LED with TiO_2 IO and reference structure, respectively.

The calculated far-field patterns of extracted light for random dipole sources are shown in **Figure 4**a. All the far-field patterns clearly show the six-fold rotational symmetry that comes from the hexagonal lattice of the IO monolayer. Each structure shows a very different far-field pattern depending on the wavelength. Particularly, for the wavelength of 510 nm, there is very strong radiation to the direction perpendicular to the IO structure. The enhancement spectra with the viewing angles of ±90° and ±10° are shown in Figure 4b and c, respectively. As can be expected from the far-field patterns, it is clear that the spectra changes dramatically for different solid angles. On the other hand, in order to compare the simulated results with the measured total

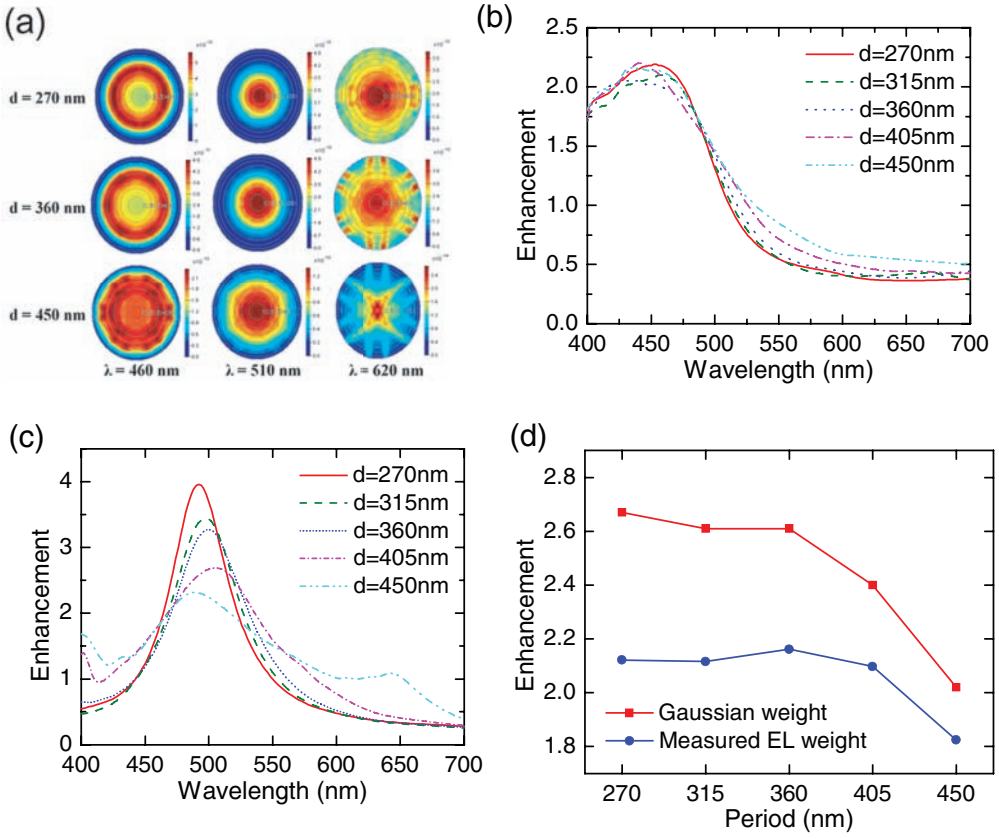

Figure 4. a) Far-field patterns of the light radiated into the air in the polymer LED with TiO_2 IO for the period d = 270, 360, 450 nm and the wavelength 460, 510, 620 nm. b) Light extraction efficiency enhancement over the viewing angle from –90° to +90°. c) Light extraction efficiency enhancement over the viewing angle from –10° to +10°. d) Light extraction efficiency enhancement for different periods of the TiO_2 IOs after weighted averaging with Gaussian spectrum and the measured EL spectrum

enhancement, we need to consider a spectral response of the light sources because the total output power changes for different light sources. Here, we firstly assume a Gaussian spectrum because the specific radiation spectrum of the reference structure is unknown. We averaged the enhancement spectra (Figure 4c) using a Gaussian weight function with the center wavelength of 510 nm and a bandwidth of 30 nm. In Figure 4d, we can see that the calculated enhancement decreases mildly as the period increases. We can also expect that 2D TiO_2 IO with the diameter of 270 nm would give the highest enhancement for the polymer LED structure with a 2D TiO_2 IO and wavelength region considered here. It is certain that LEDs with different refractive index layers or different thickness of size would show different characteristic as in Lee et al.[22] After measuring the output spectrum of the polymer LED without 2D TiO_2 IO, we added the weighted average power calculated using the normalized EL intensity spectrum in Figure 4d.

Polymer LED with insertion of the 2D TiO_2 IO between the glass and anode electrode, as shown in Figure 3a, was fabricated using glass with and without the 270 nm 2D TiO_2 IO with closed top-surface structure. Here, poly(3,4-ethylenedioxy thiophene):poly(styrene sulfonate) (PEDOT:PSS) formulation Baytron PH 500, provided by H. C. Starck, was employed as a polymer anode, as it was recently reported as an alternative anode to replace indium tin oxide (ITO) in organic LEDs.[25] An organic electrode offers the advantage of easy fabrication and can also planarize the surface roughness of the 2D TiO_2 IO with closed top-surface structure as a buffer layer. Because of the flat surface of the 2D TiO_2 IO, it is convenient to form a thin flat organic anode even by spin-coating and avoid having organic materials infiltrate into the air void. The emissive layer was spin-coated using a blend of poly(*N*-vinyl-carbazole) (PVK) and 2-(4-biphenylyl)-5-(4-*tert*-butylphenyl)-1,3,4-oxadiazole (PBD) doped with *fac*-tris(2-phenylpyridine)iridium [$Ir(ppy)_3$]. For the cathode electrode, aluminum was thermally evaporated.

Figure 5 shows the device performance of the polymer LEDs with and without the insertion of the 2D TiO_2 IO structure between the glass and anode electrode, which were measured in the direction normal to the sample surface for a solid angle of ±10°. Figure 5b, showing luminance versus voltage characteristics of the fabricated polymer LEDs with and without the structure, confirms the effectiveness of the structure for enhancing light extraction with almost the same current density as that shown in the inset of Figure 4c. The luminance of the polymer LED with the 2D TiO_2 IO was increased by 92% as compared with the reference device without the structure. The principle of the light extraction enhanced LED with the 2D PhC has been explained like this: the 2D PhC suppresses the waveguided loss by creating a photonic bandgap or diffracting the waveguided light.[11,26] Here, the 2D IO works for diffracting the waveguide light which is trapped in the anode electrode and the glass. The diffracted light escapes out of the device, which leads to an increase of the light extraction from the polymer LEDs. Figure 5b shows the normalized electroluminescence (EL) spectra of polymer LEDs with and without the 2D TiO_2 IO. Considering that the maximum enhancement peak is located at the wavelength of around 495 nm as shown in Figure 4c, the EL spectrum with 2D TiO_2 IO showing decreased intensity at the longer wavelength than 510 nm matched reasonably well with simulation data.

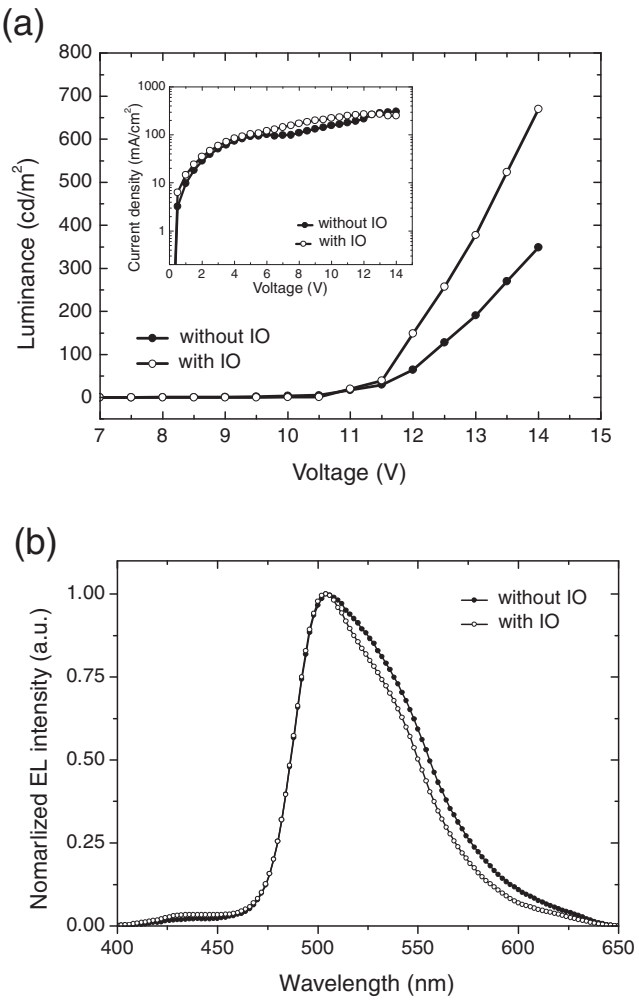

Figure 5. a) Luminance versus voltage characteristics for the polymer LEDs with and without 2D TiO_2 IO (inset: current density versus voltage characteristics for the samples). b) Normalized EL spectra of the devices. The luminance and the EL spectra are for the solid angle of –10° to +10° from the normal direction.

In summary, we successfully fabricated 2D TiO_2 IOs with a closed top-surface structure that has a thin flat layer on top. The effectiveness of the 2D TiO_2 IO structure as a 2D PhC pattern on the light extraction was demonstrated through 3D-FDTD simulation. By inserting the 2D TiO_2 IO with closed top-surface structure between the glass and the anode electrode, the light extraction of the polymer LED was enhanced by 92% without change in the electrical properties, compared with conventional devices. This enhancement is mainly due to diffraction of waveguided light by the 2D TiO_2 IO acting as 2D PhC. We believe that the 2D IO with closed top-surface structure demonstrated in this study could be applied to various types of LEDs and other optical devices for enhancing light extraction.

Experimental Section

Preparation of the TiO_x Sol Solution: To prepare the TiO_x sol solution, 16 g of titanium tetra isopropoxide (TTIP) was dropped into 16 g of

methanol in a round flask and 3.2 g of glacial acetic acid was then added into the solution at room temperature. After 30 min, 1 g of deionized water was dropped into the solution and the reaction allowed to proceed for 24 h.[27]

Fabrication of the Polymer LEDs: To prepare the anode, PH 500 containing 5% dimethylsulfoxide (DMSO) was mixed with methanol in a volume ratio of 1:1 and spin-coated onto precleaned and O_2-plasma treated 2D TiO_2 IO glass at 1 500 rpm for 30 s and heated at 120 °C for 20 min to remove residual solvent. After repeating the process twice more, a 100 nm thick polymer anode was obtained. For the emissive layer, the PVK, PBD and $Ir(ppy)_3$ were mixed in a 46:46:8 weight ratio and dissolved in chlorobenzene to make a 10 mg mL^{-1} solution. Then, the solution was spin-coated onto the 2D TiO_2 IO with closed top-surface structure at 700 rpm for 40 s for the 50 nm thick emissive layer. After annealing at 80 °C for 10 min, aluminium was thermally evaporated to deposit a cathode with a thickness of 100 nm. The active area of the devices was 2×2 mm^2.

Measurements: The electrical and luminescence characteristics of the devices were analyzed with a current and voltage-source measurement unit (Keithley 236) and a luminance meter (Minolta, LS-100). EL spectra were measured using a fluorospectroscope (ISS PC1 Photon Counter Meter). The solid angle for the detector in the experiment was ±10° around the normal direction.

3D-FDTD simulations: Each dipole was a Gaussian pulse with a center frequency of 588.9 THz and a bandwidth of 321.2 THz in frequency domain. For each sample, 29 simulations were performed including the simulation for reference structure. By applying the near-field to far-field transformation to the electric field at the monitor plane, far-field patterns were calculated for every dipole sources. A perfect electric conductor boundary condition is used in the aluminium cathode and perfectly matched layers are used for the other five boundaries.

Acknowledgements

The authors thank Prof. H. Y. Park, Korea Advanced Institute of Science and Technology, and Dr. C.-S. Kee, Advanced Photonics Research Institute, for assistance with the FDTD simulations. This work was supported by an ERC grant of the National Research Foundation of Korea NRF) funded by the Korea Ministry of Education, Science and Technology (MEST) (No. R11–2007-045–01002-0(2009)).

Received: December 20, 2010
Published online: March 7, 2011

[1] B. W. D'Andrade, S. R. Forrest, *Appl. Phys. Lett.* **2003**, *83*, 3858.
[2] Y. Sun, N. C. Giebink, H. Kanno, B. Ma, M. E. Thompson, S. R. Forrest, *Nature* **2006**, *440*, 908.
[3] G. Gu, D. Z. Garbuzov, P. E. Burrows, S. Venkatesh, S. R. Forrest, M. E. Thompson, *Opt. Lett.* **1997**, *22*, 396.
[4] A. Chutinan, K. Ishihara, T. Asano, M. Fujita, S. Noda, *Org. Electron.* **2005**, *6*, 3.
[5] P. A. Hobson, S. Wedge, J. A. E. Wasey, I. Sage, W. L. Barnes, *Adv. Mater.* **2002**, *14*, 1393.
[6] S. Möller, S. R. Forrest, *J. Appl. Phys.* **2002**, *91*, 3324.
[7] T. Yamasaki, K. Sumioka, T. Tsutsui, *Appl. Phys. Lett.* **2000**, *76*, 1243.
[8] T. Tsutsui, M. Yahiro, H. Yokogawa, K. Kawano, M. Yokoyama, *Adv. Mater.* **2001**, *13*, 1149.
[9] Y. R. Do, Y. C. Kim, Y.-W. Song, C.-O Cho, H. Jeon, Y.-J. Lee, S.-H. Kim, Y.-H. Lee, *Adv. Mater.* **2003**, *15*, 1214.
[10] M. F. Fujita, K. Ishihara, T. Ueno, T. Asano, S. Noda, H. Ohata, T. Tsuji, H. Nakada, N. Shimoji, *Jpn. J. Appl. Phys.* **2005**, *44*, 3669.
[11] A. M. Adawi, R. Kullock, J. L. Turner, C. Vasilev, D. G. Lidzey, A. Tahraoui, P. W. Fry, D. Gibson, E. Smith, C. Foden, M. Roberts, F. Qureshi, N. Athanassopoulou, *Org. Electron.* **2006**, *7*, 222.
[12] J. E. G. T. Wijnhoven, W. L. Vos, *Science* **1998**, *281*, 802.
[13] R. C. Schroden, M. Al-Daoes, C. F. Blanford, A. Stein, *Chem. Mater.* **2002**, *14*, 3305.
[14] P. Lodahl, A. Floris van Driel, I. S. Nikolaev, A. Irman, K. Overgaag, D. Vanmaekelbergh, W. L. Vos, *Nature* **2004**, *430*, 654.
[15] Z. Yang, X. Huang, L. Sun, J. Zhou, G. Yang, B. Li, C. Yu, *J. Appl. Phys.* **2009**, *105*, 083523.
[16] J. K. Kim, T. Gessmann, E. F. Schubert, J.-Q. Xi, H. Luo, J. Cho, C. Sone, Y. Park, *Appl. Phys. Lett.* **2006**, *88*, 013501.
[17] A. Taflove, S. C. Hagness, *Computational Electrodynamics: the Finite-Difference Time-Domain Method*, Artech House, Norwood, MA **2000**.
[18] J. H. Kim, M. Chainey, M. S. El-Aasser, J. W. Vanderhoff, *J. Polym. Sci., Part A: Polym. Chem.* **1992**, *30*, 171.
[19] M. H. Kim, S. H. Im, O. O. Park, *Adv. Funct. Mater.* **2005**, *15*, 1329.
[20] M. H. Kim, H. K. Choi, O. O. Park, S. H. Im, *Appl. Phys. Lett.* **2006**, *88*, 143127.
[21] Y. Cao, Y. Wang, Y. Zhu, H. Chen, Z. Li, J. Ding and Y. Chi, *Superlattice Microstruct.* **2006**, *40*, 155.
[22] Y.-J. Lee, S.-H. Kim, J. Huh, G.-H. Kim, Y.-H. Lee, S.-H. Cho, Y.-C. Kim, Y. R. Do, *Appl. Phys. Lett.* **2003**, *82*, 3779.
[23] W. J. Choi, Q.-H. Park, D. Kim, H. Jeon, C. Sone, Y. J. Park, *J. Korean Phys. Soc.* **2006**, *49*, 877.
[24] H. Greiner, J. Pond, presented at the 9th Int. Conf. Near-Field Opt., Nanophotonics and Relat. Techniques, Lausanne, Switzerland, September 2006.
[25] K. Fehse, K. Walzer, K. Leo, W. Lövenich, A. Elschner, *Adv. Mater.* **2007**, *19*, 441.
[26] A. David, T. Fujii, R. Sharma, K. McGroddy, S. Nakamura, S. P. DenBaars, E. L. Hu, C. Weisbuch, H. Benisty, *Appl. Phys. Lett.* **2006**, *88*, 061124.
[27] D. H Wang, S. H. Im, H. K. Lee, O. O. Park, J. H. Park, *J. Phys. Chem. C* **2009**, *113*, 17268.